Geophysical Research Letters

RESEARCH LETTER
10.1029/2024GL112554

M_2 Seasonal Variability in Northwestern Europe: Characteristics and Drivers

Lucia Pineau-Guillou[1] and **Pascal Lazure**[1]

[1]IFREMER, Laboratoire d'Océanographie Physique et Spatiale, UMR 6523 (IFREMER, CNRS, IRD, UBO), IUEM, Brest, France

Key Points:

- M_2 displays a strong seasonal cycle in the North Sea with amplitude larger than 5 cm
- The seasonality is well reproduced by a barotropic model forced with the tidal potential and the atmosphere only
- The seasonal cycle is mainly due to gravitational nonlinear effects in a large part and atmospheric effects in a smaller extent

Correspondence to:

L. Pineau-Guillou,
lucia.pineau.guillou@ifremer.fr

Citation:

Pineau-Guillou, L., & Lazure, P. (2025). M_2 seasonal variability in northwestern Europe: Characteristics and drivers. *Geophysical Research Letters*, *52*, e2024GL112554. https://doi.org/10.1029/2024GL112554

Received 13 SEP 2024
Accepted 20 JAN 2025

Abstract The M_2 tide displays large seasonal variability in Europe, particularly in the North Sea. The tide is there larger in summer than in winter. However, there is no consensus on the physical drivers leading to such large values, atmosphere circulation and stratification being two good candidates. We analyzed hourly sea level data from observations at 35 tide gauges in Europe. The amplitude of M_2 seasonal cycle is the largest in the southern North Sea, reaching typically 4–6 cm. This cycle is well reproduced by a barotropic model, forced with the tidal potential and the atmosphere only. This suggests a minor role of the stratification. We show that large seasonal cycles in the southern North Sea are first due to gravitational nonlinear effects. The atmosphere also plays a role, but locally and in a smaller extent.

Plain Language Summary The tide is changing over a year, the amplitude of the tide being larger in summer than in winter in the North Sea. We try here to understand what are the reasons that explain such changes over a year. For this purpose, we analyze sea level data from 35 tide gauges in Europe. We found that the largest changes occur in the southern North Sea. Such changes are well reproduced by a model, whose inputs are the tidal potential and the atmosphere only, and which does not consider the stratification of the waters. This means that the stratification only plays a minor role. We show that the tide changes over a year, first because of the gravitational tide (some nonlinear components introducing some seasonal modulations). The atmosphere also plays a role, but locally and in a smaller extent.

1. Introduction

The tide refers to the cyclic variations of the sea level, from "gravitational" origin (due to the gravitational forces of the Moon and Sun), but also from "radiational" origin (due to cyclic meteorological effects) (Simon, 2007, 2013). Gravitational components come directly from the tidal potential (e.g., M_2) or from their interactions generating harmonics (e.g., M_4, M_6). Radiational components come from seasonal meteorological cycles such as the annual cycle in atmospheric pressure (e.g., S_a). Gravitational and radiational contributions to tide are often difficult to disentangle, as both may occur at the same frequency, as for instance for S_2 (Ray, 2009). (Note that our terminology for "gravitational" and "radiational" tide is in line with Simon (2007, 2013), but slightly different from Ray (2022), who considers as "gravitational" only tidal components that are in the tidal potential—and not their nonlinear interactions. As soon as we define the gravitational tide as the sea level's response to the gravitational forcing, our approach makes sense.)

Tide is changing at centennial scale, for non astronomical reasons (Haigh et al., 2022; Ray & Talke, 2019; Woodworth, 2010). Over the last century, tidal constituents typically changed from 1 to 10 cm (Müller et al., 2011; Pineau-Guillou et al., 2021; Ray & Talke, 2019). The causes of observed changes may be local (e.g., deepening of channels, Familkhalili & Talke, 2016) or from large-scale origin. Many physical processes are possible drivers, such as changes in water levels due to sea level rise or ground movements (Idier et al., 2017; Pickering et al., 2017; Schindelegger et al., 2018), changes in the atmospheric circulation (Challis et al., 2023; Pineau-Guillou et al., 2021), changes in the ocean stratification that will modify internal tides and bottom friction (Müller, 2012; Opel et al., 2024), changes in the radiational forcing (Ray, 2009) or changes in the extent of sea-ice cover (Haigh et al., 2022).

Tide is also changing at seasonal scale (Müller et al., 2014; Ray, 2022; Tazkia et al., 2017). The main difference between centennial and seasonal changes, is that seasonal changes can be due to astronomical constituents (Ray, 2022), although these are rarely mentioned as drivers (compared to physical drivers such as meteorological forcing, river discharges, ice coverage or stratification, e.g., Müller et al., 2014). Various studies already

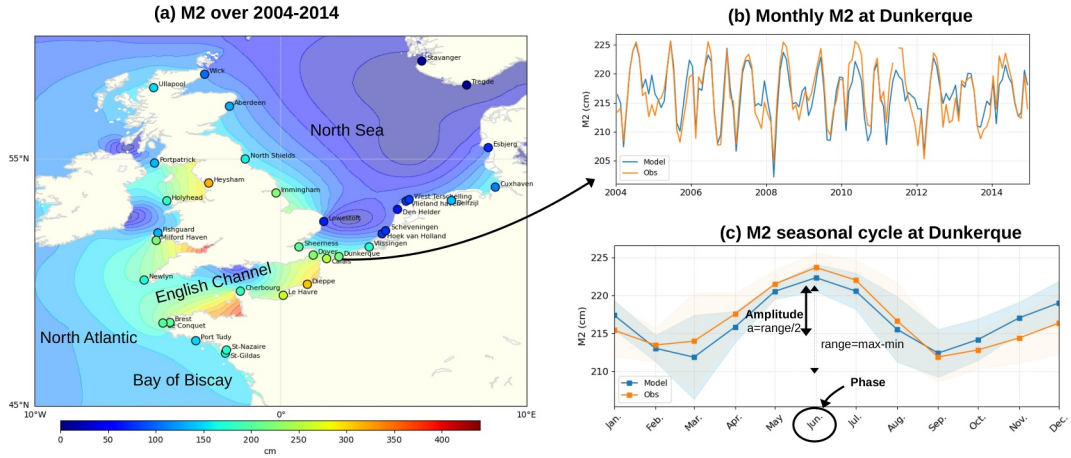

Figure 1. (a) M_2 computed over 2004–2014 from observations (colored dots) and model (filled contours), (b) monthly M_2 at Dunkerque observed (orange) and modeled (blue), and (c) M_2 seasonal cycle at Dunkerque observed (orange) and modeled (blue). The seasonal amplitude is defined as half of the range of the seasonal cycle, the range being the difference between the maximum and minimum M_2 over the year. The seasonal phase is defined as the month where the M_2 amplitude is maximum. The shaded areas correspond to the $\pm 1\sigma$ confidence interval.

investigated M_2 seasonal variability at global and regional scale, for example, Müller et al. (2014) globally, Tazkia et al. (2017) in the Bay of Bengal, Devlin et al. (2018) in southeast Asian waters, Huess and Andersen (2001) and Gräwe et al. (2014) in the North Sea. Despite all agree that tide displays a strong seasonality, with amplitude larger than 5 cm in the North Sea (Gräwe et al., 2014), and up to 25 cm in Bangladesh (Ray, 2022), there is no consensus on the physical drivers leading to observed changes in certain regions. In particular in the North Sea, some studies invoke a major role of the atmospheric circulation (Huess & Andersen, 2001), and consider the seasonality as a barotropic phenomenon, whereas others suggest a predominant role of the stratification (Gräwe et al., 2014; Müller et al., 2014) considering that the seasonality is largely a baroclinic process. Recently, Opel et al. (2024) who investigated the role of stratification on tide globally, reported that possibly, competing processes might be at work in the North Sea.

The present paper aims at understanding the physical drivers of M_2 seasonal variability in Europe (English Channel and the North Sea). We first analyze sea level observations at 35 tide gauges to characterize the amplitude and phase of M_2 seasonal cycle. We then run a barotropic model, to understand which physical drivers lead to large amplitudes, particularly in the southern North Sea.

Note that we here focus on the seasonality of the amplitude of M_2, and not its phase. This work is therefore a first step, as changes in phase may also be significant (1.5° in average), leading to potential elevations of a few cm.

2. Data and Method

2.1. Sea Level Observations

We used 35 tide gauges (Figure 1a) from Global Extreme Sea Level Analysis (GESLA-3) sea level data set (Caldwell et al., 2015; Haigh et al., 2022; Woodworth et al., 2017). This data set provides 5,119 records of high-frequency (mainly hourly) sea level observations around the world. We selected the coastal stations located in the North-East Atlantic (from 45°N to 60°N and from 15°W to 10°E) with at least 50 years of data. We discarded tide gauges that were not representative of the open ocean (3 stations in the Netherlands, Den Oever buiten, Kornwerderzand buiten and Harlingen), without recent data (2 stations, Southampton record in the UK ends in 1990 and Ijmuiden Noordersluis in the Netherlands ends in 1983) or with doubtful data (1 station, Hellevoetsluis in the Netherlands, reported as "not research quality data" in the Permanent Service for Mean Sea Level website). This led to consider 35 tide gauges. Hourly sea level data were extracted over the period 2004–2014 (period of our study) at these 35 stations.

2.2. Ocean Numerical Model

We used the global ocean model TUGO (Lyard et al., 2006). This model in barotropic mode resolves the classical shallow water continuity and momentum equations. This numerical model is particularly adapted to investigate tide, as it is used to develop the FES2014 global ocean tide atlas (Lyard et al., 2021) and to correct satellite altimeter data from tide and atmospheric effects (Carrère & Lyard, 2003). Note that there is no stratification in the model (barotropic mode). We used the default TUGO model configuration, with the FES2014 unstructured grid (Lyard et al., 2021). The grid resolution varies from 15 km offshore to 2 km in nearshore areas (see Figure 5 in Pineau-Guillou et al. (2020) for a grid illustration). The model is forced by the tidal potential and by the winds and atmospheric pressure. Those atmospheric data come from Twentieth Century Reanalysis Version 3 (Slivinski et al., 2019), a 3 hr and 1° atmospheric data set (0.5° for the native grid) over 1836–2015.

We conducted simulations over 2004–2014 (period of our study). Outputs are the hourly sea levels at the 35 tide gauges (nearest grid point in the native grid), and hourly sea levels on a 0.05° grid (around 5 km resolution). We conducted two simulations: one forced with the tidal potential only (referred as "tide only" on figures), the other forced with the tidal potential and the atmosphere (referred as "tide + atm" on figures).

2.3. Computation of M_2 Seasonal Cycle

To compute the M_2 seasonal cycle at the 35 stations, we processed the 2004–2014 hourly sea level data (observed and modeled). In a first step, we computed M_2 each month, using Utide tidal analysis software (Codiga, 2011). Nodal modulations were carefully empirically removed (more details in Appendix A from Pineau-Guillou et al. (2021)). Only months with sufficient data (more than 75%) were considered. We then obtain monthly M_2 time series over 2010–2014 (see Figure 1b for an example at Dunkerque, France). In a second step, we averaged all the monthly values, to estimate the seasonal cycle over a year and its associated standard deviation (see Figure 1c for an example, still in Dunkerque). The seasonal cycle is characterized by its seasonal amplitude and phase, defined as follows. The seasonal amplitude is half of the range of the seasonal cycle, the range being the difference between the maximum and minimum M_2 over a year. The seasonal phase is the month where the M_2 amplitude is maximum over a year (see Figure 1c for an illustration).

2.4. Computation of Tidal Atlases

To compute atlases of harmonic constituents on the whole area (M_2 on Figure 1a and other constituents on Figure 4), we analyzed simulations over 2004–2014 with the Tidal ToolBox (Allain, 2021), which has been specifically developed for this purpose.

Finally, note that the average M_2 (i.e., computed over the whole period 2004–2014) may differ between the model and observations (see the discrepancies on Figure 1a, Root Mean Square Error of 14.7 cm). For this reason, M_2 from the model was bias corrected $\left(M_{2mod}(t) = M_{2mod}(t) - \overline{M_{2mod}(t)} + \overline{M_{2obs}(t)}\right)$, when plotted on figures (Figures 1b, 1c, 2e, and 3b). This ensures an easier visual comparison between the observed and modeled seasonal cycles.

3. Results and Discussion

3.1. M_2 Seasonal Cycle

We analyzed the 2004–2014 observed and modeled sea level data, to compute the M_2 seasonal cycle amplitude (observed Figure 2a, modeled Figure 2b) and phase (observed Figure 2c, modeled Figure 2d). Some examples of M_2 seasonal cycle over a year are displayed at 4 stations (Figure 2e), whose name are labeled on Figure 2d to show their locations. The main result is that the model correctly reproduces the seasonal cycle, whereas it is only forced by the tidal potential and the atmosphere (no stratification). More details are given in the following.

The observed amplitude of the seasonal cycle is of 3.3 cm in average at the 35 stations (Figure 2a), and ranges from 0.5 to 6.7 cm depending on the station. The eastern and northern Europe display small amplitudes (minimum of 0.5 cm at Stavanger, Norway), whereas the eastern English Channel and the southern North Sea display large amplitudes, typically more than 4 cm (maximum of 6.7 cm at Delfzijl, Netherlands). In these areas of large values, the seasonal cycle is maximum in June (Figure 2b).

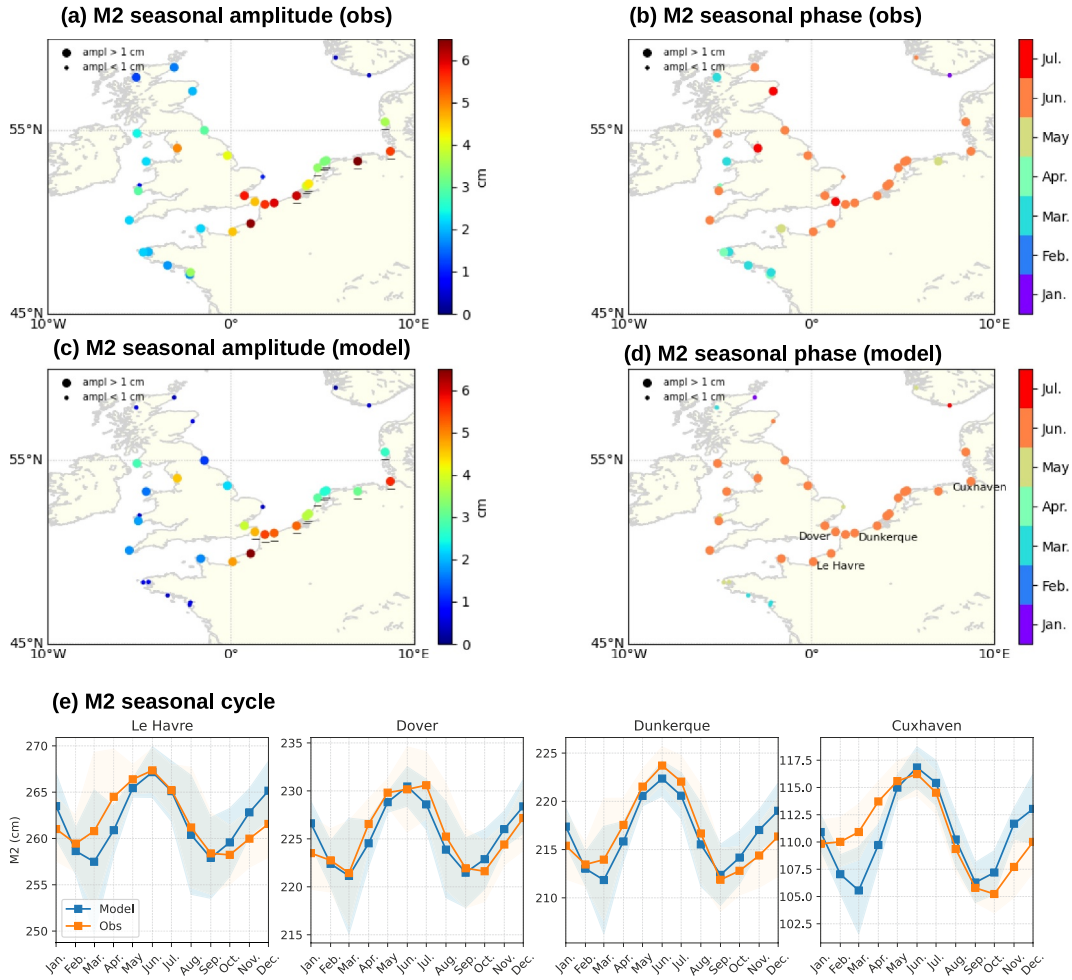

Figure 2. M_2 seasonal amplitude from (a) observations and (c) model. M_2 seasonal phase from (b) observations and (d) model. (e) M_2 seasonal cycle at Le Havre, Dover, Dunkerque, and Cuxhaven. Note that these four stations are labeled on panel (d). At the underlined stations on panels (a, c), the main frequencies are annual and semi-annual, when applying a Fast Fourier Transform analysis on monthly M_2 time series (see Figure 1b for an example of monthly M_2 time series).

Overall, the model well reproduces the amplitude of the seasonal cycle (Figure 2c), with similar high values in the eastern English Channel (e.g., 4.8 cm at Le Havre, vs. 4.6 cm for the observations) and in the southern North Sea (e.g., 5.6 cm at Cuxhaven against 5.5 cm for the observations). However, the amplitude is overall underestimated

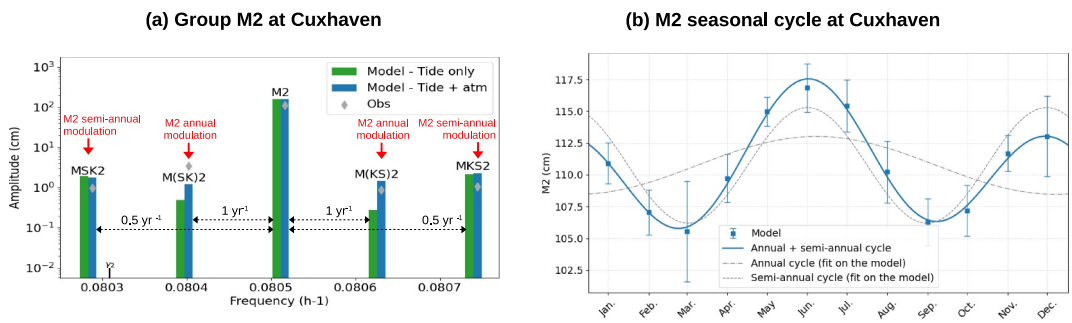

Figure 3. (a) Group M_2 at Cuxhaven obtained from harmonic analysis of the model with tide only (green) and with tide and atmosphere (blue) over 2004–2014, using the Tidal Toolbox. The same for observations (gray diamonds). M_2 is modulated semi-annually by MSK_2 and MKS_2 and annually by $M(SK)_2$ and $M(KS)_2$. The names are in line with Simon (2007, 2013) (see Table 1). Note that γ_2 is schematically represented, but ignored in the Tidal Toolbox due to its very low value in the tidal potential (b) M_2 seasonal cycle from the model at Cuxhaven, with a fit of an annual and semi-annual cycle.

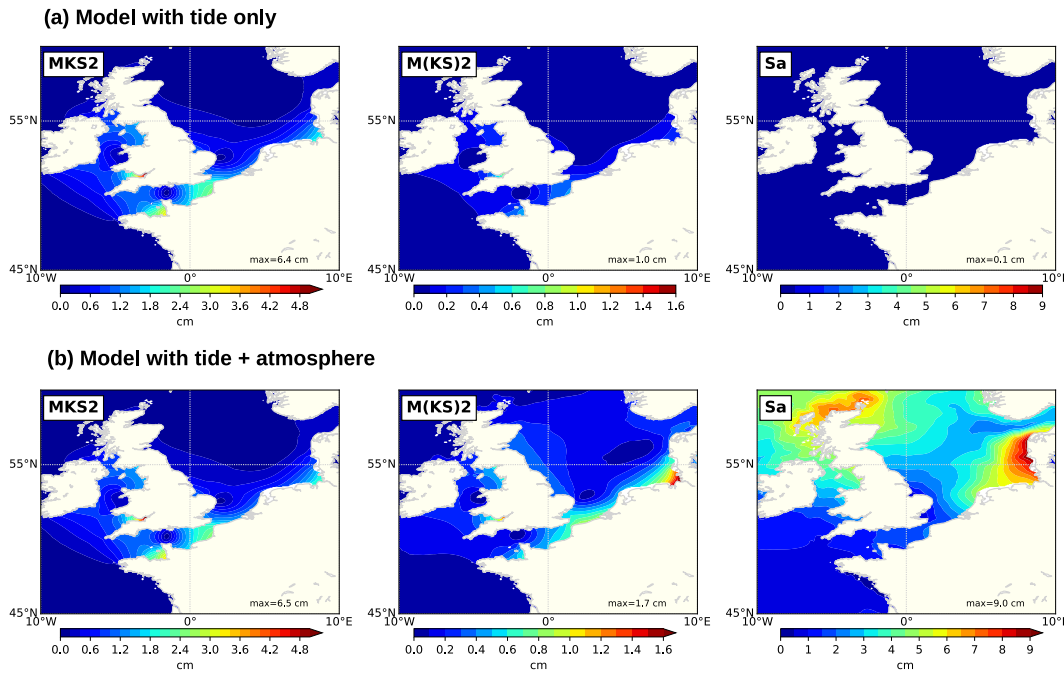

Figure 4. Amplitude of MKS_2, $M(KS)_2$, and Sa obtained from harmonic analysis of the model with (a) tide only and (b) tide and atmosphere over 2004–2014.

by the model (average amplitude of 2.5 cm against 3.3 cm for the observations), particularly at Delfzijl (Netherlands) in the southern North Sea (3.1 cm for the model against 6.7 cm for the observations). Note that this station, located in the Ems estuary, is surrounded by a chain of islands, which makes it difficult to model. The model also well reproduces the phase of the seasonal cycle (maximum in June in the English Channel and the North Sea), except for some stations. Note that for stations with small amplitude (less than 1 cm, see the small dots on Figure 2c) the phase is not relevant, as there is almost no seasonal cycle.

Beyond the amplitude and phase, the whole M_2 seasonal cycle over a year is generally correctly modeled, as illustrated on Figure 2e for 4 stations with large amplitude (more than 4 cm). Again, the maximum in June is correctly reproduced by the model. However, a small shift of around 15 days appears sometimes between the model and the observations, in March and November (see for example Le Havre on Figure 2e). This is possibly due to missing processes in the model (see the discussion further).

3.2. Physical Drivers

The model, which is only forced by the tidal potential and the atmosphere, correctly reproduces the observed seasonal cycle. This suggests that these two processes (tidal potential and atmosphere) explain most of the seasonal cycle. We remind that there is no effect of stratification, as we use a barotropic model. In the following, we will analyze more deeply the M_2 monthly time series, to understand the origin of the M_2 seasonal cycle.

We first applied a Fast Fourier Transform on the monthly M_2 time series (observed and modeled) at each of the 35 stations, to detect the frequencies of the M_2 seasonal cycle (see Figure 1b for an example of monthly M_2 time series). We found that monthly M_2 time series major frequencies are annual and semi-annual in southern North Sea (see the underlined stations on Figures 2a and 2c). Interestingly, these stations are also those with the largest seasonal amplitude. In fact, at these stations, the seasonal cycle can be correctly represented with an annual and a semi-annual fit, as illustrated at Cuxhaven (Germany) on Figure 3b. But what are the origins of these annual and semi-annual components?

These annual and semi-annual modulations of M_2 are due to neighboring components in M_2 group (see the example of Cuxhaven, based on a harmonic analysis of the model over 2004–2014, Figure 3a, in complement to Figure 1 from Ray (2022)). Note that in the present paper, the constituent names are in line with Simon (2007, 2013) and current international conventions (from International Hydrographic Organization) and displayed

Table 1
Harmonic Constituents Characteristics in the M_2 Group

Names	Other names	q (°/h)	Doodson	Argument	Origin
MSK_2	MSK_2	28.901967	2 535 555	$2\tau - 2h$	Interaction $q_{MSK2} = q_{M2} + q_{S2} - q_{K2}$
	No name	28.901967	2 535 555	$2\tau - 2h$	Interaction $q_{noname} = q_{M2} - q_{Ssa}$
	OP_2	28.901967	2 535 557	$2\tau - 2h + \pi$	Interaction $q_{OP2} = q_{O1} + q_{P1}$
γ_2	GAM_2	28.911251	2 537 557	$2\tau - 2h + 2p + \pi$	Tidal potential ($a = 0.00300$)
$M(SK)_2$	$M(SK)_2$	28.943036	2 545 554	$2\tau - h - \frac{\pi}{2}$	Interaction $q_{M(SK)2} = q_{M2} + (q_{S1} - q_{K1})$
	MA_2	28.943036	2 545 555	$2\tau - h$	Interaction $q_{MA2} = q_{M2} - q_{Sa}$
	α_2 or H_1	28.943038	2 545 567	$2\tau - h + p_1 + \pi$	Tidal potential ($a = 0.00345$)
M_2	M_2	28.984104	2 555 555	2τ	Tidal potential ($a = 1$)
	KO_2	28.984104	2 555 557	$2\tau + \pi$	Interaction $q_{KO2} = q_{K1} + q_{O1}$
$M(KS)_2$	$M(KS)_2$	29.025173	2 565 556	$2\tau + h + \frac{\pi}{2}$	Interaction $q_{M(KS)2} = q_{M2} + (q_{K1} - q_{S1})$
	MB_2	29.025173	2 565 555	$2\tau + h$	Interaction $q_{MB2} = q_{M2} + q_{Sa}$
	β_2 or H_2	29.025171	2 565 545	$2\tau + h - p_1$	Tidal potential ($a = 0.00305$)
MKS_2	MSK_2	29.066242	2 575 555	$2\tau + 2h$	Interaction $q_{MKS2} = q_{M2} + q_{K2} - q_{S2}$
	No name	29.066242	2 575 555	$2\tau + 2h$	Interaction $q_{noname} = q_{M2} + q_{Ssa}$
	δ_2	29.066242	2 575 555	$2\tau + 2h$	Tidal potential ($a = 0.0015$)

Note. Names (column 1) are in line with Simon (2007, 2013). Constituents with other names (column 2) can not be separated from the main name (column 1), as their frequencies are the same, because they only differ by the 6th Doodson number (mean longitude of the solar perigee p_1, whose period is 20,9 centuries) or by the 7th Doodson number (multiple of $\pi/2$). For the origin of the constituents (column 6), a is the relative amplitude of the component compared to M_2 in the tidal potential.

Table 1 (column 1). Other names may appear in the literature (column 2), depending on the tidal analysis software or the authors. For example, the following names refer to the same tidal frequency: $M(SK)_2$ in the Tidal Toolbox (Allain, 2021), MA_2 in Ray (2022) or H_1 in Utide software (Codiga, 2011). Surprisingly, MSK_2 does not appear in Utide software, and signs at γ_2 frequency. Note that the nodal constituent m_2 is not mentioned in Table 1 (or displayed on Figure 3a), because it introduces an 18.6 years modulation of M_2 which is not in the scope of the present paper. Figure 3a illustrates that 1 year of data is required to correctly separate M_2 from its two neighboring components $M(SK)_2$ and $M(KS)_2$ (as their frequencies differ from 1 year), and 6 months is needed to correctly separate M_2 from MSK_2 and MKS_2. As a consequence, with monthly analysis, M_2 is modulated by these neighboring components, annually and semi-annually.

To understand the origin (tide or atmosphere?) of these neighboring components, we conducted a harmonic analysis of the model forced with tide only or forced with both tide and atmosphere. Amplitudes are displayed at Cuxhaven on Figure 3a, and on the whole study area on Figure 4 (note that only $M(KS)_2$ and MKS_2 are displayed, atlases being very similar for $M(SK)_2$ and MSK_2 due to the symmetry of the M_2 group, see Figure 3a). We found that the semi-annual modulation components MSK_2 and MKS_2 are clearly of gravitational origin. Indeed, the simulation with tide only or with both tide and atmosphere give similar amplitudes (2 cm at Cuxhaven Figure 3a and up to 6 cm elsewhere Figures 4a and 4b). The picture is different for the annual modulation components $M(SK)_2$ and $M(KS)_2$. These components are small in the simulation with tide only (0.5 and 0.3 cm at Cuxhaven respectively, Figures 3a and 4a), but they are enhanced when the atmosphere is added (1.2 and 1.6 cm at Cuxhaven respectively, Figures 3a and 4b). The atmosphere acts through the annual component S_a, a radiational component only due to the atmosphere (amplitude close to 0 for the model with tide only Figure 4a, but up to 9 cm for the model with both tide and atmosphere Figure 4b). Once generated, this S_a component interacts with M_2, and the resulting components (sometimes referred as MA_2 and MB_2 in the literature) are exactly at the frequency of $M(SK)_2$ and $M(KS)_2$, which explains the enhancement of these components with the atmosphere forcing.

To go further, the reader can refer to Table 1, which details the origin of the components of the M_2 group and underlines the complexity to disentangle the drivers. At the same frequency, components of different origin overlap. (Note that components in the column entitled "Other names" can not be separated from components in the column "Names," as their frequencies are the same, see the figure caption for more details). At the same

frequency, components may come directly from the tidal potential, or result from interactions between purely gravitational components, or between gravitational and radiational components. For example, at the frequency of $M(KS)_2$, three components overlap: (a) β_2 which comes directly from the tidal potential, (b) $M(KS)_2$ which comes from the interaction between M_2, K_1 and S_1, (c) MB_2 which comes from the interaction between M_2 and S_a (as explained previously). Note that the picture is even more complex, as the atmosphere not only play a role in MB_2, but also in $M(KS)_2$, as S_1 is partly radiational (but very small, S_1 is smaller than 0.8 cm in the simulation with tide only, and smaller than 1.7 cm in the simulation with tide and atmosphere). Finally, the contribution that comes directly from the tidal potential (α_2, β_2, γ_2, and δ_2) is quite small, that is, always smaller than 0.3% of M_2 (see the value of a in Table 1), which means for example, around 0.5 cm at Cuxhaven. Note that the gravitational $M(KS)_2$ (Figure 4a middle panel) mainly comes from the tidal potential (i.e., linear origin), as β_2 alone would lead to amplitudes close to those of $M(KS)_2$ (around 0.5 cm). Finally, note that only part of possible nonlinear interactions are listed in Table 1, as many others may occur at a given frequency (e.g., $M_2 + S_2 - T_2$ matches with $M(KS)_2$ frequency).

To resume, in the southern North Sea, the seasonal cycle is mainly due to gravitational nonlinear effects (in a large part) and atmospheric effects (in a smaller extent). However, some small discrepancies between the model and observations suggest that other processes may also play a role. In the model, the semi-annual and annual cycle are both maximum in June, which explains the strong amplitude in the North Sea (see Figure 3b). Differently, in the observations, the annual cycle seems to be slightly shifted earlier in the year (maximum rather in May, not shown), the semi-annual cycle being still in June. This may explain the observed shift of around 15 days around March and November, when comparing the modeled and observed seasonal cycles (Figure 2e). These discrepancies are possibly due to physical processes that are omitted in the model. Our barotropic model only captures the atmospheric-induced annual cycle, which is likely underestimated in some areas (e.g., at Cuxhaven, see observed and modeled $M(SK)_2$ on Figure 3a), as we are missing the baroclinic-induced annual cycle, due for example, to the summer stratification (e.g., in the North Sea). Despite this, the model well catches the overall seasonal cycle, as in most of the areas, the seasonal effect is dominated by the semi-annual modulation (e.g., in the southern English Channel, where MKS2 reaches 2–3 cm, against less than 1 cm for M(KS)2, see Figure 4b). Discrepancies between observations and the model may also come from some limitations of the model, including uncertainties on input data or parameterizations, but also its poor resolution (only 2 km in nearshore areas). This resolution might not be sufficient to correctly capture the fine-scale nearshore dynamics, in complex areas such as the North Sea, with tidal inlets and sand banks.

4. Conclusion

We analyzed hourly sea level data from observations and simulations at 35 tide gauges to characterize M_2 seasonal cycle. We found strong amplitudes in the southern North Sea, typically from 4 to 6 cm, M_2 being maximum in June. A barotropic model forced only with the tidal potential and the atmosphere correctly reproduces this cycle.

We analyzed simulations forced with tide only and with both tide and atmosphere, to understand the origin of the large amplitudes in the southern North Sea. We found that the seasonal cycle was mainly due to annual and semi-annual modulation of M_2 from neighboring nonlinear components. Whereas the semi-annual modulation is from gravitational origin, the annual modulation is partly from gravitational origin, and enhanced by the atmosphere. This enhancement may exceed 1 cm locally.

To conclude, Huess and Andersen (2001) partly anticipated these results almost 25 years ago, reporting that the seasonal tide was mainly a barotropic phenomena in the North Sea, due first to "non linear combination between the tidal frequencies" and with "a dependency on the meteorological field over the area." In the present paper we went further, explaining which constituents interact and to what extent.

In future modeling studies investigating the tide seasonality, we recommend to systematically run the model with tide only, to first estimate which part of the seasonality is due to gravitational components. Once this part is determined, an analysis of the frequencies of M_2 monthly time series should help to understand the other drivers. Note that any change in the sea level annual cycle (S_a), whether due to annual cycle in atmospheric pressure, large river discharges or stratification, will enhance the seasonality.

Data Availability Statement

The GESLA-3 sea level data set (Caldwell et al., 2015; Haigh et al., 2022; Woodworth et al., 2017) analyzed during the current study is available on the GESLA website, https://gesla787883612.wordpress.com/downloads/. The 20CR (Twentieth Century Reanalysis) Version 3 atmospheric data (Slivinski et al., 2019) are available on the 20CR website https://psl.noaa.gov/data/20thC_Rean/. Support for the Twentieth Century Reanalysis Project version 3 data set is provided by the U.S. Department of Energy, Office of Science Biological and Environmental Research (BER), by the National Oceanic and Atmospheric Administration Climate Program Office, and by the NOAA Physical Sciences Laboratory. The Utide tidal analysis software (Codiga, 2011) is available on the Utide website, https://pypi.org/project/UTide/.

Acknowledgments
This research has been supported by the French National Research Agency (ANR) Grant ClimEx (ANR-21-CE01-0004). We thank Florent Lyard from LEGOS (Laboratoire d'Etudes en Géophysique et Océanographie Spatiales, France) for providing the FES2014 unstructured grid (Lyard et al., 2021) and the TUGO software (https://sirocco.obs-mip.fr/ocean-models/tugo/).

References

Allain, D. (2021). TUGOm tidal Toolbox. Tech. rep., LEGOS Documentation. Retrieved from http://ftp.legos.obs-mip.fr/pub/ecola/tools/ttb.pdf

Caldwell, P. C., Merrifield, M. A., & Thompson, P. R. (2015). Sea level measured by tide gauges from global oceans — The joint archive for sea level holdings (NCEI accession 0019568), version 5.5 [Dataset]. *NOAA National Centers for Environmental Information*. https://doi.org/10.7289/V5V40S7W

Carrère, L., & Lyard, F. (2003). Modeling the barotropic response of the global ocean to atmospheric wind and pressure forcing-comparisons with observations. *Geophysical Research Letters*, *30*(6), 1275. https://doi.org/10.1029/2002GL016473

Challis, J., Idier, D., Wöppelmann, G., & André, G. (2023). Atmospheric wind and pressure-driven changes in tidal Characteristics over the northwestern European shelf. *Journal of Marine Science and Engineering*, *11*(9), 1701. https://doi.org/10.3390/jmse11091701

Codiga, D. (2011). *Unified tidal analysis and prediction using the UTide Matlab functions ( )*. Technical Report 2011-01 (p. 59). Graduate School of Oceanography, University of Rhode Island.

Devlin, A. T., Zaron, E. D., Jay, D. A., Talke, S. A., & Pan, J. (2018). Seasonality of tides in southeast Asian waters. *Journal of Physical Oceanography*, *48*(5), 1169–1190. https://doi.org/10.1175/JPO-D-17-0119.1

Familkhalili, R., & Talke, S. A. (2016). The effect of channel deepening on tides and storm surge: A case study of Wilmington. NC. *Geophysical Research Letters*, *43*(17), 9138–9147. https://doi.org/10.1002/2016GL069494

Gräwe, U., Burchard, H., Müller, M., & Schuttelaars, H. M. (2014). Seasonal variability in M2 and M4 tidal constituents and its implications for the coastal residual sediment transport. *Geophysical Research Letters*, *41*(15), 5563–5570. https://doi.org/10.1002/2014GL060517

Haigh, I. D., Marcos, M., Talke, S. A., Woodworth, P. L., Hunter, J. R., Hague, B. S., et al. (2022). GESLA version 3: A major update to the global higher-frequency sea-level dataset. *Geoscience Data Journal*, *10*(3), 1–22. https://doi.org/10.1002/gdj3.174

Huess, V., & Andersen, O. B. (2001). Seasonal variation in the main tidal constituent from altimetry. *Geophysical Research Letters*, *28*(4), 567–570. https://doi.org/10.1029/2000GL011921

Idier, D., Paris, F., Cozannet, G. L., Boulahyaa, F., & Dumas, F. (2017). Sea-level rise impacts on the tides of the European Shelf. *Continental Shelf Research*, *137*, 56–71. https://doi.org/10.1016/j.csr.2017.01.007

Lyard, F., Allain, D. J., Cancet, M., Carrère, L., & Picot, N. (2021). FES2014 global ocean tide atlas: Design and performance. *Ocean Science*, *17*(3), 615–649. https://doi.org/10.5194/os-17-615-2021

Lyard, F., Lefevre, F., Letellier, T., & Francis, O. (2006). Modelling the global ocean tides: Modern insights from FES2004. *Ocean Dynamics*, *56*(5–6), 394–415. https://doi.org/10.1007/s10236-006-0086-x

Müller, M. (2012). The influence of changing stratification conditions on barotropic tidal transport and its implications for seasonal and secular changes of tides. *Continental Shelf Research*, *47*, 107–118. https://doi.org/10.1016/j.csr.2012.07.003

Müller, M., Arbic, B. K., & Mitrovica, J. X. (2011). Secular trends in ocean tides: Observations and model results. *Journal of Geophysical Research*, *116*(C5), C05013. https://doi.org/10.1029/2010JC006387

Müller, M., Cherniawsky, J. Y., Foreman, M. G. G., & von Storch, J. S. (2014). Seasonal variation of the M2 tide. *Ocean Dynamics*, *64*(2), 159–177. https://doi.org/10.1007/s10236-013-0679-0

Opel, L., Schindelegger, M., & Ray, R. (2024). A likely role for stratification in long-term changes of the global ocean tides. *Communications Earth & Environment*, *5*(1), 261. https://doi.org/10.1038/s43247-024-01432-5

Pickering, M. D., Horsburgh, K. J., Blundell, J. R., Hirschi, J. J.-M., Nicholls, R. J., Verlaan, M., & Wells, N. (2017). The impact of future sea-level rise on the global tides. *Continental Shelf Research*, *142*, 50–68. https://doi.org/10.1016/j.csr.2017.02.004

Pineau-Guillou, L., Bouin, M.-N., Ardhuin, F., Lyard, F., Bidlot, J.-R., & Chapron, B. (2020). Impact of wave-dependent stress on storm surge simulations in the North Sea: Ocean model evaluation against in situ and satellite observations. *Ocean Modelling*, *154*, 101694. https://doi.org/10.1016/j.ocemod.2020.101694

Pineau-Guillou, L., Lazure, P., & Wöppelmann, G. (2021). Large-scale changes of the semidiurnal tide along North Atlantic coasts from 1846 to 2018. *Ocean Science*, *17*(1), 17–34. https://doi.org/10.5194/os-17-17-2021

Ray, R. D. (2009). Secular changes in the solar semidiurnal tide of the western North Atlantic. *Geophysical Research Letters*, *36*(19), L19601. https://doi.org/10.1029/2009GL040217

Ray, R. D. (2022). Technical note: On seasonal variability of the M2 tide. *Ocean Science*, *18*(4), 1073–1079. https://doi.org/10.5194/os-18-1073-2022

Ray, R. D., & Talke, S. A. (2019). Nineteenth-century tides in the Gulf of Maine and implications for secular trends. *Journal of Geophysical Research: Oceans*, *124*(10), 7046–7067. https://doi.org/10.1029/2019JC015277

Schindelegger, M., Green, J. A. M., Wilmes, S., & Haigh, I. D. (2018). Can we model the effect of observed sea level rise on tides? *Journal of Geophysical Research: Oceans*, *123*(7), 4593–4609. https://doi.org/10.1029/2018JC013959

Simon, B. (2007). *La marée océanique côtière*. Institut Océanographique Ed. Retrieved from https://iho.int/iho_pubs/CB/C-33/C-33_maree_simon_fr.pdf

Simon, B. (2013). *Coastal tides*. Institut Océanographique Ed. Retrieved from https://iho.int/iho_pubs/CB/C-33/C-33_maree_simon_en.pdf

Slivinski, L. C., Compo, G. P., Whitaker, J. S., Sardeshmukh, P. D., Giese, B. S., McColl, C., et al. (2019). Towards a more reliable historical reanalysis: Improvements for version 3 of the Twentieth century reanalysis system. *Quarterly Journal of the Royal Meteorological Society*, *145*(724), 2876–2908. https://doi.org/10.1002/qj.3598

Tazkia, A., Krien, Y., Durand, F., Testut, L., Islam, A. S., Papa, F., & Bertin, X. (2017). Seasonal modulation of M2 tide in the northern Bay of Bengal. *Continental Shelf Research*, *137*, 154–162. https://doi.org/10.1016/j.csr.2016.12.008

Woodworth, P. L. (2010). A survey of recent changes in the main components of the ocean tide. *Continental Shelf Research*, *30*(15), 1680–1691. https://doi.org/10.1016/j.csr.2010.07.002

Woodworth, P. L., Hunter, J. R., Marcos, M., Caldwell, P., Menéndez, M., & Haigh, I. (2017). Towards a global higher-frequency sea level dataset. *Geoscience Data Journal*, *3*(2), 50–59. https://doi.org/10.1002/gdj3.42